J Mol Med
DOI 10.1007/s00109-016-1437-9

JMolMed CrossMark

ORIGINAL ARTICLE

A molecular imaging biosensor detects in vivo protein folding and misfolding

Anjali V. Sheahan[1] · **Thillai V. Sekar**[1] · **Kai Chen**[1] · **Ramasamy Paulmurugan**[1] · **Tarik F. Massoud**[1]

Received: 13 March 2016 / Revised: 8 May 2016 / Accepted: 2 June 2016

Abstract
Aberrant protein folding represents the molecular basis of many important human diseases. Although the discovery of new anti-misfolding drugs is a major priority in molecular therapeutics, there is currently no generalizable protein folding assay for use in cell-based high throughput screening (HTS) of chemical libraries, or for in vivo imaging. We molecularly engineered a bioluminescence-based biosensor composed of rationally split Firefly luciferase reporter fragments flanking a test protein, and used this in a protein-fragment complementation assay to quantitatively measure folding of the test protein. We comprehensively validated this biosensor in vitro, in cells, and by optically imaging protein folding and misfolding in living mice using several test proteins including enhanced green fluorescent protein, Renilla luciferase, Gaussia luciferase, and SIRT1. Applications of this novel biosensor are potentially far-reaching in both cell-based HTS approaches to discover new anti-misfolding drugs, and when using the same biosensor in validation studies of drug candidates in small animal models.

Key messages
- Novel anti-misfolding drugs are needed as molecular therapeutics for many diseases.
- We developed first in vivo imaging protein folding biosensor to aid drug discovery.
- Biosensor created by flanking a test protein with rationally split Firefly luciferase.
- Biosensor validated by detecting folding of test proteins EGFP, Rluc, Gluc, and SIRT1.
- Generalizable molecular biosensor for translational applications in drug screening.

Keywords Protein folding · Protein misfolding · Molecular imaging · Drug discovery · High throughput screening · Bioluminescence imaging

Electronic supplementary material The online version of this article (doi:10.1007/s00109-016-1437-9) contains supplementary material, which is available to authorized users.

✉ Ramasamy Paulmurugan
paulmur8@stanford.edu

✉ Tarik F. Massoud
tmassoud@stanford.edu

[1] Laboratory of Experimental and Molecular Neuroimaging, Molecular Imaging Program at Stanford (MIPS), and Bio-X Program, Stanford University School of Medicine, Stanford, CA 94305-5427, USA

The discovery of small molecule drugs that hinder the formation of misfolded protein conformations, and which may ultimately lead to the prevention of misfolding disease phenotypes, is a major goal in molecular therapeutics [1, 2]. Currently, rational drug design based on knowledge of protein structural biology, or high throughput screening (HTS) of chemical libraries, provides platforms for discovery of potential novel pharmacologically active anti-misfolding drugs.

Numerous in vitro biophysical experimental tools have been created to advance our understanding of protein folding mechanisms [3]. A variety of approaches to analyze protein folding and their stability are available in vitro, but they require purified protein and do not allow assessment of protein stability within the cellular environment. In cell culture, the most common general approaches are to examine component protein stability using subsequent western blot or pulse-chase analysis, but such methods are not amenable to high-throughput studies [4]. In the past few years, several in vivo

Published online: 08 June 2016

stability reporters have also been developed, including the study of protein fusion with GFP, α-complementation of β-galactosidase, and split versions of GFP and β-lactamase (reviewed in [4]). The latter two reporters used an insertional approach, where a target protein was inserted directly into a reporter, reducing false positives owing to proteolysis or initiation of protein translation at internal sites, which can untether the reporter from the target protein [5]. Using a similar insertional approach, Pittman et al. [4] described a folding assay (intra-dihydrofolate reductase enzyme stability assay, IDESA) that was designed for high-throughput use and where protein stability is coupled to cell proliferation in the model yeast, *Saccharomyces cerevisiae*. They demonstrated its use with a range of disease-relevant targets, to identify stabilizing small molecules (pharmacological chaperones) for unstable alleles.

Of several "single cell" techniques to study protein folding, such as FlAsH dye-labeling and NMR spectroscopy (reviewed in Ebbinghaus et al. [6]), fluorescence resonance energy transfer (FRET) has been used for many years to study folding and unfolding of proteins at a single molecule level and in live cells by probing the distances between fluorescent donor and acceptor molecules attached to the termini [7], or within domains [8], of test proteins. The strong distance dependence ($1/R^6$) of the FRET rate constant allows the measurement of distances on the 2 to 8 nm scale, between donor and acceptor labels on a biomolecule [9]. Thus, FRET can provide a reaction coordinate that provides a global view of conformational distributions and dynamics of a protein as it folds [10]. Furthermore, a feature of FRET is that it can be used to image the fast dynamics of biomolecules in vivo with subcellular resolution. For example, fast relaxation imaging (FReI) couples time-resolved FRET imaging with fast temperature jump-induced kinetics to measure reversible fast folding kinetics as well as protein folding thermodynamics inside a single living cell with high spatiotemporal resolution [6]. Unfortunately, fluorescence reflectance imaging in living animals is decidedly surface-weighted when compared to bioluminescence imaging [11]. Therefore, a particular advantage of bioluminescence over fluorescence is that its use could be extrapolated to preclinical mouse model imaging using the same reporter-based molecular construct during subsequent optical imaging validation studies of promising drug candidates [12]. Knowing that most fully folded native proteins have N- and C-termini in close spatial proximity (average distance of 2.7 nm) [13], we modeled our new bioluminescence-based biosensor on the stereospecific requirements for FRET in folding studies, to quantitatively measure protein folding or misfolding using bioluminescence imaging.

Here we describe the molecular engineering rationale (see further discussion in Supplementary Material), construction, and validation of this novel biosensor based on a chimeric molecular construct of rationally split Firefly luciferase (Fluc) reporter fragments [14] flanking a test protein (Fig. 1a), used in a protein-fragment complementation assay (PCA) [15, 16] to measure and indirectly quantitate [17] the extent of protein folding or misfolding in mammalian cells using luminometry studies in cell lysates, and for bioluminescence imaging of these live cells in culture and subcutaneous implants in living mice. We used several test proteins including enhanced green fluorescent protein (EGFP), Renilla luciferase (Rluc), Gaussia luciferase (Gluc), and SIRT1. Importantly, the split-Fluc fragments used in this study had been shown previously [18] to not exhibit self- or unassisted complementation when expressed in cells. Thus, fully functional Fluc is restored only upon complementation that is assisted by proper protein folding. This strategy is generalizable and has the potential for applications in the basic study of protein folding in vivo, and translational applications in diverse molecular imaging cell-based HTS platforms aimed at discovery of novel or repurposed anti-misfolding drugs for many important diseases.

Materials and methods

Expression vectors

We obtained all restriction and ligase enzymes and appropriate buffers from New England Biolabs (Ipswich, MA). We used the five PRIME Taq DNA Polymerase kit (Fisher Scientific, Pittsburgh, PA) for PCR reactions with primers generated at

Fig. 1 Design and characterization of the protein folding biosensor. **a** Schematic of the strategy to assay protein folding status. Complementation of NFluc and CFluc fragments results in restoration of Fluc enzymatic function upon proper folding of the attached protein of interest (ribbon diagram of GFP, as an example). **b** Assessment of EGFP as a test protein by differential interference contrast (*DIC*) bright field microscopy and EGFP fluorescence imaging of HEK293T cells transiently expressing wtEGFP and its split-Fluc fusion (*wtEGFP-fusion*). Untransfected cells were a negative control (*Negative*). **c** GFP median fluorescence intensity (MFI in relative fluorescence units [RFU]) in the corresponding live cell populations by flow cytometry, gated to include only GFP positive cells. **d** Western blot shows differential expression of wtEGFP and wtEGFP-fusion proteins in lysates collected from these cells. **e** Results of FACS analysis upon normalization with western blot data. **f** Assessment of Fluc fragment orientation on EGFP function by DIC bright field microscopy and GFP fluorescence imaging of HEK293T cells transiently expressing NFluc-wtEGFP-CFluc (*wtEGFP-fusion*) or the reverse orientation CFluc-wtEGFP-NFluc (*wtEGFP-rev*) fusion proteins. Untransfected cells were a negative control. **g** Western blot shows relatively equal protein expression levels in lysates obtained from the corresponding cell populations. **h** EGFP MFI in live wtEGFP-fusion and wtEGFP-rev expressing cell populations by flow cytometry, gated to include only EGFP positive cells. **i** Normalized Fluc bioluminescence measurements from lysates of wtEGFP-fusion and wtEGFP-rev expressing cells. **j** Normalized Fluc bioluminescence measurements from live wtEGFP-fusion and wtEGFP-rev expressing cells. *$P = 0.01$–0.05; **$P = 0.001$–0.01; ***$P < 0.001$; *ns* not significant

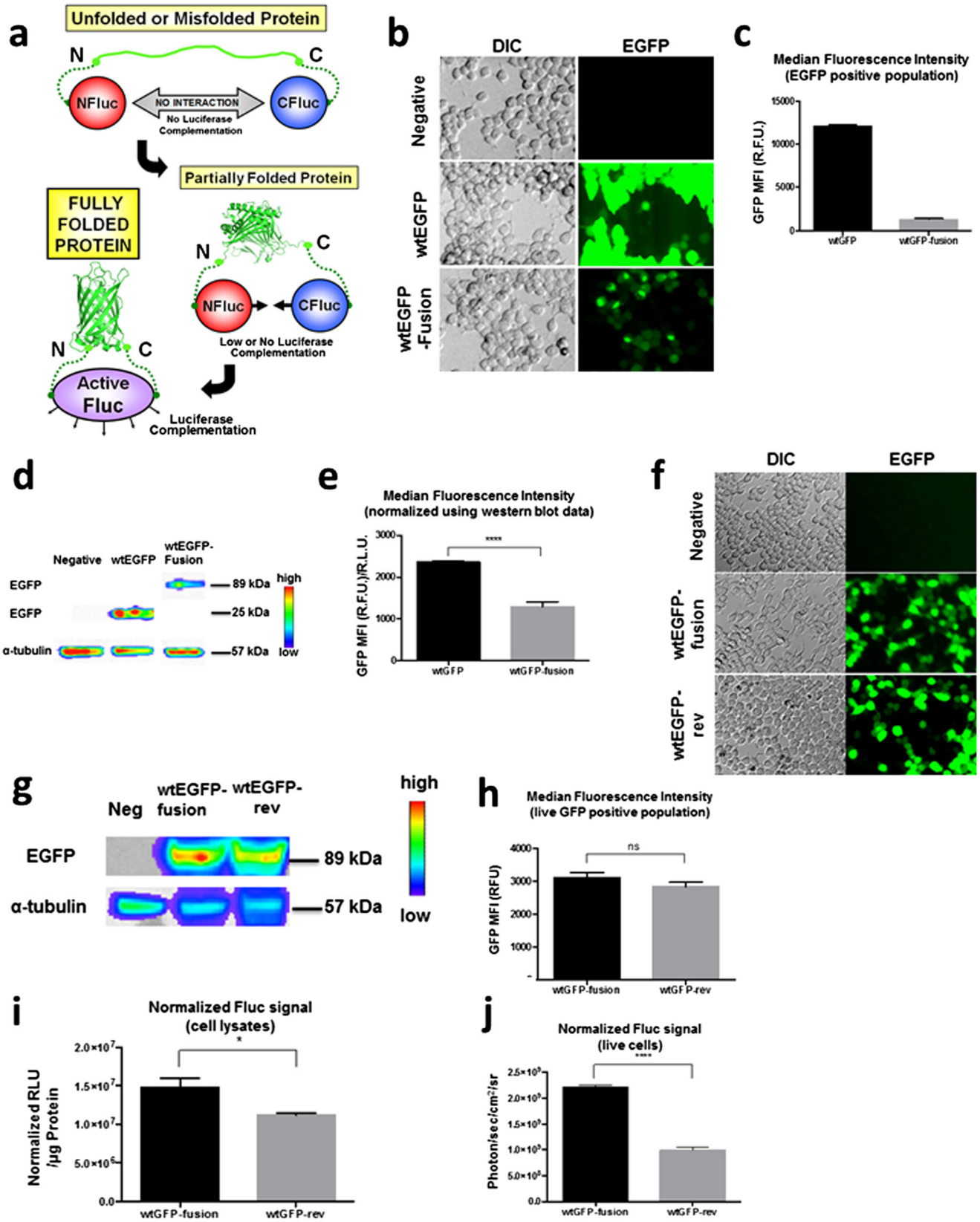

the Protein and Nucleic Acid Facility (Stanford School of Medicine). A list of primers is available upon request.

We generated constructs using an in-house plasmid (pcPuro) produced by modifying the pcDNA3.1(+) plasmid

(Life Technologies, Grand Island, NY) so that it expressed the puromycin resistance gene instead of the neomycin resistance gene. A schematic representation of all vector constructs employed in this study is shown in Supplementary Fig. (1). We verified all plasmid vector constructs by enzymatic digestion as well as sequencing (Sequetech, Mountain View, CA). Details of generating vectors for wild-type EGFP, EGFP variants, Renilla luciferase, Gaussia luciferase, truncated Gaussia luciferase, and wild-type and mutant SIRT1 are presented in the Supplementary Material.

Cell culture

Cell lines were obtained from the American Type Culture Collection (ATCC, Manassas, VA) and cell culture reagents were purchased from Life Technologies (Grand Island, NY). Human embryonic kidney (HEK293T) cells and a human lung carcinoma cell line (A549) were maintained in Dulbecco's Modified Eagle's Medium (Cat #: 11995) supplemented with 10 % fetal bovine serum and 1 % penicillin/streptomycin. We performed transient transfections on cultures when they were 80 % confluent using the Lipofectamine 2000 transfection reagent. Plasmid DNA-Lipofectamine 2000 complexes were prepared according to manufacturer's instructions in Opti-MEM Reduced Serum Medium. We used 1.5 μL of Lipofectamine 2000 for every microgram of plasmid DNA.

Determination of luciferase activity in cell lysates

HEK293T and A549 cells were seeded in triplicate in 24-well plates using cell-seeding concentrations of 7.5×10^4 and 5×10^4 cells/well, respectively. After 24 h, we transiently transfected each well with 0.5 μg of plasmid. Where indicated, cells were co-transfected with 0.5 ng of the RLuc expression vector to provide a transfection efficiency control. Each well was harvested after 48 h under non-denaturing conditions with 100 μL ice-cold 1× Passive Lysis Buffer (Promega, Madison, WI), after which plates were placed on an orbital shaker for 10 min to further facilitate cell lysis. We then collected cell lysates and centrifuged them at 10,000 rpm at 4 °C for 5 min to remove cell debris.

A 20/20n luminometer (Turner Biosystems, Sunnyvale, CA) was used for FLuc and RLuc bioluminescence measurements. We prepared a 10-μL sample of cleared supernatant, which was assayed for FLuc activity by the addition of 50 μL LARII substrate (Promega, Madison, WI). We assayed a second 10-μL sample of cleared supernatant for RLuc activity by the addition of 50 μL of coelenterazine (Nanolight, Pinetop, AZ).

We employed the Bio-Rad Protein Assay (Bio-Rad, Hercules, CA) to determine protein concentration. Briefly, 5 μL samples of cleared supernatant were added to each well of a 96-well plate, to which 100 μL of diluted dye reagent was added, prepared according to manufacturer's instructions. After a 5-min room-temperature incubation, we measured absorbance at 595 nm using an Infinite M1000 PRO microplate reader (Tecan, San Jose, CA). We normalized FLuc activity with RLuc activity as well as total protein in the analysis of data generated to correct for transfection efficiency and cell lysis efficiency, respectively.

Determination of EGFP fluorescence in cell lysates

We also used cell lysates, prepared when determining luciferase activity, to determine EGFP fluorescence. We dispensed a 40-μL sample of each lysate to a well of a 96-well plate. The plate was then read using a 488-nm excitation wavelength and a 508–510-nm emission wavelength using an Infinite M1000 PRO microplate reader (Tecan, San Jose, CA). We normalized EGFP fluorescence with RLuc activity as well as total protein to correct for transfection efficiency and cell lysis efficiency, respectively.

Determination of luciferase activity in live cells

HEK293T and A549 cells were seeded in triplicate in 24-well plates using cell-seeding concentrations of 7.5×10^4 and 5×10^4 cells/well, respectively. We prepared two sets of 24-well plates for bioluminescence measurements. After 24 h, we transiently transfected each well with 0.5 μg of plasmid. Where indicated, cells were co-transfected with 0.5 ng of the RLuc expression vector to provide a transfection efficiency control. After 48 h, we removed media from one set of plates, which was then assayed for FLuc activity by the addition of 200 μL of D-luciferin (Biosynth, Itasca, IL) into each well. The second set of plates was assayed for RLuc activity by the addition of 200 μL coelenterazine (Nanolight, Pinetop, AZ) into each well. We acquired measurements by bioluminescence imaging using the IVIS-Lumina imaging system (Perkin Elmer, Waltham, MA). We normalized EGFP fluorescence with RLuc activity to correct for transfection efficiency.

Determination of EGFP fluorescence in live cells

HEK293T and A549 cells were seeded in six-well plates using cell-seeding concentrations of 3×10^5 and 2×10^5 cells/well, respectively. After 24 h, we transiently transfected each well with 2 μg of EGFP construct. After 48 h, EGFP fluorescence and DIC bright field images were collected using an Olympus IX81 motorized inverted microscope. We then collected cells by trypsinization, centrifugation in complete media, and resuspension of the cell pellet in 1 mL of phosphate-buffered saline (PBS). We analyzed 100 μL of this cell suspension, diluted up to 1 mL with PBS, for EGFP fluorescence by flow cytometry (FACS Aria III, BD Biosciences, San Jose, CA).

Data was analyzed using the FlowJo FACS Analysis software. The remaining 900 μL of cell suspension was pelleted by centrifugation and set aside for western blot analysis.

Evaluation of SIRT1 function in cell lysates

We used a fluorometric SIRT1 Activity Assay Kit (Abcam, Cambridge, MA) to detect SIRT1 activity in lysates. Sample preparation and assays were according to the manufacturer's instructions. Briefly, HEK293T cells were seeded in 10 cm tissue culture dishes using a cell-seeding concentration of 1.8×10^6 cells/dish. After 24 h, we transiently transfected each well with 2 μg of SIRT1-fusion or SIRT1 (R446E)-fusion plasmid. Each well was harvested after 48 h under non-denaturing conditions with 100 μL ice-cold 1× lysis buffer (prepared in accordance with the SIRT1 Activity Assay protocol booklet). We sonicated this cell suspension four times for 5 s each on ice after which samples were centrifuged at 10, 000 rpm at 4 °C for 5 min to remove cell debris. We isolated SIRT1 protein from 200 μL of supernatant by immunoprecipitation as follows: We incubated the samples with 10 μg anti-Fluc antibody (sc-57604, Santa Cruz Biotechnology, Santa Cruz, CA). We then added this sample to a 50-μL preparation of Dynabeads Protein A for Immunoprecipitation (Life Technologies, Carlsbad, CA) and placed this mixture on a rotating mixer for 20 min at 4 °C. Dynabeads were isolated by magnetic separation. We washed the beads three times on ice with 500 nL of 1× lysis buffer and once with 500 μL of SIRT1 assay buffer (component of SIRT1 Activity Assay Kit). Following magnetic separation of the Dynabeads and aspiration of the wash buffer, we added reaction mixture containing Fluoro-Substrate peptide solution (component of SIRT1 Activity Assay Kit) to the Dynabeads and measured NAD-dependent deacetylase activity according to the procedure outlined in the manufacturer's instructions for the SIRT1 Activity Assay Kit.

Western blot analysis

HEK293T and A549 cells were seeded in six-well plates using cell-seeding concentrations of 3×10^5 and 2×10^5 cells/well, respectively. After 24 h, we transiently transfected each well with 2 μg of plasmid. Cells were harvested in 100 μL RIPA lysis buffer (Pierce Biotechnology). We also lysed any cell pellets collected in 100 μL RIPA lysis. Protein concentration was determined using the 660-nm Protein Assay (Pierce Biotechnology) according to the manufacturer's instructions. We prepared protein samples, containing 10 μg of total protein in 1× Lamelli loading buffer with β-mercaptoethanol (Life Technologies, Carlsbad, CA), which were denatured at 100 °C for 5 min, resolved on 4–12 % SDS-polyacrylamide pre-cast gels (Life Technologies, Carlsbad, CA) and electroblotted onto a polyvinylidene difluoride nylone membrane (Bio-Rad, Hercules, CA). We used the SeeBlue Pre-Stained Standard (Life Technologies, Carlsbad, CA) to enable molecular weight estimations. Membranes were blocked in 5 % non-fat dry milk in Tris-buffered saline containing 0.01 % Tween-20 (TBST) followed by incubation with a primary antibody. As appropriate, we used antibodies suitable for the detection of EGFP (600-101-215, Rockland antibodies & assays, Limerick, PA), Gluc (#E8023S, New England Biolabs, Ipswich, MA), Rluc (ab185925, Abcam, Cambridge, MA), or Fluc (sc-57604, Santa Cruz Biotechnology, Santa Cruz, CA). Following three TBST washes, we incubated membranes with the appropriate horseradish-peroxidase conjugated secondary antibody (Sigma Aldrich). After three additional TBST washes, we incubated immunoblots with the Pierce ECL Western Blotting Substrate (Thermo Scientific, Waltham, MA) for 1 min, and then used the IVIS-Lumina imaging system (Caliper Life Sciences, Hopkington, MA) to detect and measure chemiluminescent bands. An α-tubulin primary antibody (B-5-1-2, Santa Cruz Biotechnology, Santa Cruz, CA) was used as a loading control antibody.

Generation of stable cell lines

We generated HEK293T cells stably expressing the wtEGFP-fusion and EGFP (T66K, G68C)-fusion proteins as follows: We seeded two 10 cm tissue culture dishes using a cell-seeding concentration of 1.8×10^6 cells/dish. After 24 h, one dish was transfected with 10 μg of the wtEGFP-fusion plasmid and the other with the EGFP (T66K, G68C)-fusion expression vector. Stably transfected cells were selected by 2 weeks of cultivation in 300 ng/mL puromycin-containing complete media. Following antibiotic selection, we verified expression of fusion proteins in each of the pooled populations by western blot. We also measured FLuc signal in cell lysates and confirmed fluorescence activity by fluorescence imaging.

Animal experiments

We conducted all animal experiments with the approval of the Administrative Panel on Laboratory Animal Care (APLAC), Stanford University. We used HEK293T cells stably expressing the wtEGFP-fusion and EGFP (T66K, G68C)-fusion proteins to induce xenografts in female *nu/nu* mice (Charles River, Wilmington, MA). Western blot data was used to determine the number of cells to implant. Xenografts were generated by the subcutaneous implantation of 3×10^6 cells stably expressing the wtEGFP-fusion protein or 24×10^6 cells stably expressing the EGFP (T66K, G68C)-fusion protein, in 50 % Matrigel (BD Biosciences, San Jose, CA), into the right and left lower flanks of each animal. There were, thus, five animals in total, each bearing one wtEGFP-fusion xenograft in the left lower flank and one EGFP (T66K, G68C)-fusion

xenograft in the right lower flank (10 tumors in total, 5 per group).

In vivo Fluc bioluminescence and GFP fluorescence images were obtained 0, 1, 2, 3, and 7 days post-implantation, as well as the experimental endpoint (18 days post-implantation). We used the IVIS-Lumina imaging system (Caliper Life Sciences, Alameda, CA) to obtain FLuc bioluminescence images and measurements, following delivery of 3 mg of D-luciferin (Biosynth, Itasca, IL) in 100 μL PBS by intraperitoneal injection. EGFP fluorescence was also imaged and measured using an excitation wavelength of 500 nm and an emission wavelength of 540 nm. Tumors were harvested immediately after in vivo images were acquired and placed on a stage. These tumors were then subjected to ex vivo bioluminescence and EGFP fluorescence measurements using the IVIS-Lumina imaging system. Tumor masses were also recorded prior to storage.

Statistical analysis

All data are representative of at least three independent experiments. Histograms were prepared using Prism (GraphPad Software Inc., La Jolla, CA), which was also used to perform statistical analyses. In general, results are presented as mean ± SEM. Statistical differences between means were determined using an unpaired *t* test (for two groups) or a one-way ANOVA with Tukey's multiple comparison test (three groups or more). Results of FACS analysis are presented as median fluorescence intensity ± MAD, and the statistical significance of differences between populations was determined using a Mann–Whitney test (two groups) or the Kruskal-Wallis test with Dunn's post test (three groups or more). The SIRT1 kinetic assay was analyzed using a two-way ANOVA with Tukey's multiple comparison's test. Observations with a *P* value less than 0.05 were considered statistically significant.

Results and discussion

After initial design and construction of the biosensor, its baseline characterization, and comprehensive studies of generalizability using several test proteins (EGFP, Rluc, and Gluc) and different cell lines (Supplementary Material, Fig. 1, and Supplementary Fig. 2–6), we then examined in three sets of experiments the sensitivity and specificity of the biosensor in detecting both folding and misfolding of EGFP (see also Supplementary Material). First, we generated non-functional EGFP mutants by distorting the Threonine^{66}-Tyrosine^{67}-Glycine^{68} tripeptide sequence (corresponding to the Serine^{65}-Tyrosine^{66}-Glycine^{67} sequence of GFP) known to be critical for EGFP function [19, 20]. We constructed expression vectors for EGFP (T66K), EGFP (G68C), EGFP (T66K, G68C) proteins, and their split-Fluc fusion counterparts into the biosensors, and transiently delivered these to HEK293T cells. Taken together, the results shown in Supplementary Fig. 8 indicate that forced misfolding of the EGFP molecule, induced by residue substitutions within its functional unit, can be detected and quantified by Fluc bioluminescence measurements using this biosensor.

Second, we used circularly permuted variants of EGFP (cpEGFPs) based on cpGFPs that had been evaluated by Topell et al. previously [21]. In that study, based on spectrophotometric analysis of purified proteins expressed in *Escherichia coli*, 9 of their 20 cpGFPs were shown to fold sufficiently well to then retain the ability to form the chromophore. We thus generated 20 separate cpEGFPs using breakpoints in the molecule equivalent to those described previously. Each cpEGFP was fused at the N- and C-terminal ends with the N- and C-terminal fragments of Fluc, respectively, to construct the biosensors. Expression vectors for each cpEGFP biosensor as well as the wtEGFP-fusion expression vector were delivered to HEK293T cells. The results in Supplementary Fig. 9 show that, qualitatively, functional cpEGFP-fusion proteins with a relatively high EGFP fluorescence [cpEGFP (K159-Q158) and cpEGFP (I230-G229)] also provided a strong bioluminescence signal, thus yielding further support for a relation between EGFP fluorescence and EGFP folding-assisted complementation of Fluc.

Third, the observation that the cpEGFP variant generated using the I230-G229 breakpoint resulted in a protein that produced a fluorescent signal at levels comparable to wtEGFP led us to develop another functional mutant of EGFP that we used to further validate the biosensor. Since this cpEGFP indicated that the rearrangement of the ten C-terminal residues of EGFP to the N-terminus resulted in a functional protein, we therefore generated a truncated EGFP variant (tEGFP) containing only the first 230 amino acids of EGFP, and then delivered expression vectors for tEGFP and the tEGFP-fusion proteins to HEK293T cells to enable fluorescence and bioluminescence measurements. The results in Supplementary Fig. 10 show that, aside from establishing that the 10 C-terminal residues of EGFP have a minimal role in the functional conformation of this protein, we were, more importantly, able to confirm a relation between fluorescence and bioluminescence signal in yet another EGFP mutant.

We then determined the correlation between levels of EGFP folding-assisted Fluc complementation and its ensuing bioluminescence signal, and EGFP fluorescence (from wtEGFP-, cpEGFP-, and tEGFP-expressing live HEK293T cells), by calculating the Pearson correlation coefficients (Supplementary Fig. 11). We found a robust correlation between split-Fluc complementation (bioluminescence signal from the biosensor) and test protein folding and function (fluorescence signal), which strongly validates use of this molecular imaging biosensor to detect and quantify the folding status of the test protein EGFP.

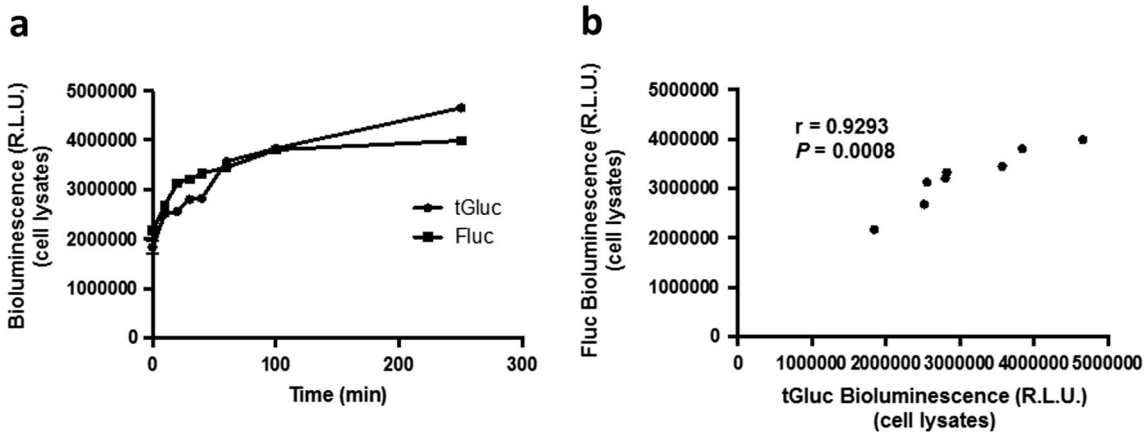

Fig. 2 Assessment of the slow folding of tGluc using the split-Fluc biosensor. **a** We observed a parallel increase in tGluc and Fluc bioluminescence measurements obtained from cell lysates, collected from HEK293T cells transiently expressing NFluc-tGluc-CFluc over a 4-h period after lysis. **b** There was a strong correlation between tGluc and Fluc bioluminescence measurements, indicating Fluc fragment complementation mirrored the nascent folding of tGluc

To also demonstrate the dynamic range of the biosensor in a system that features intermediate stages of protein folding, rather than under conditions of either fully folded or misfolded proteins (as above), we used Gluc truncated of its secretory signal peptide (tGluc) We had previously observed that removal of the secretory signal peptide of Gluc (residues 1–16) results in significant intracellular retention of protein, as well as very low activity per protein mass when assayed

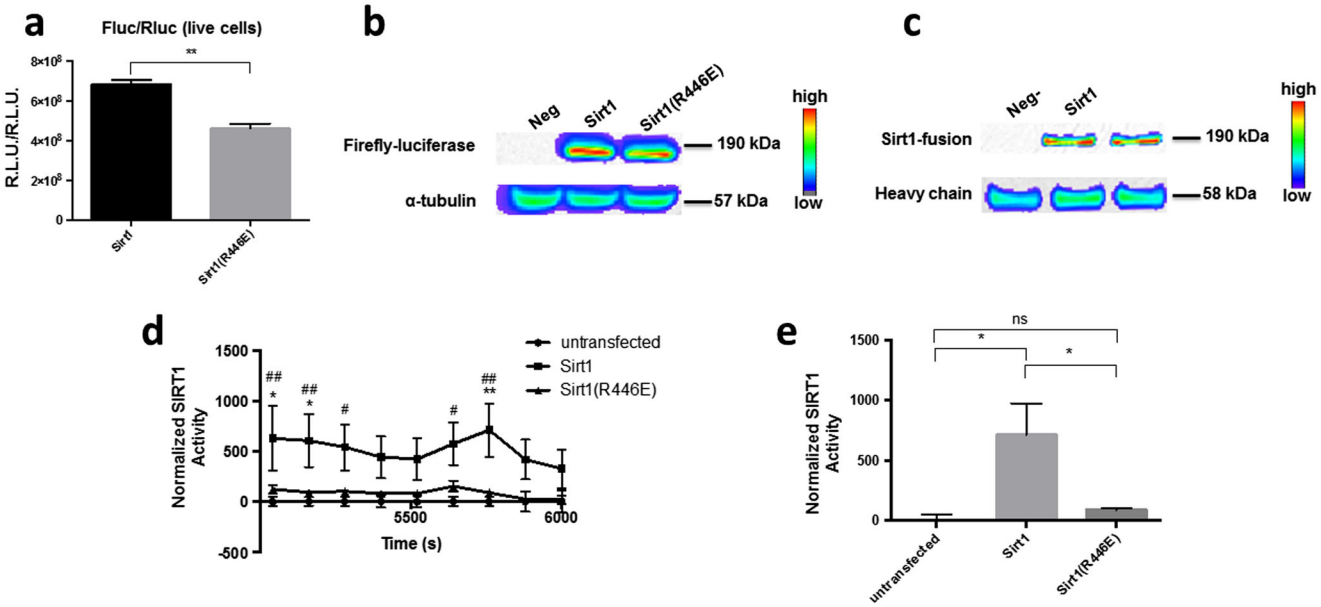

Fig. 3 Evaluation of the split-Fluc biosensor in detecting conformation of SIRT1. **a** There was a significant difference in the normalized Fluc bioluminescence obtained from SIRT1-fusion or SIRT1 (R446E)-fusion protein expressing live HEK293T cells. **b** Western blot of cell lysates showed relatively equal expression of the two fusion proteins. Untransfected cells were used as a negative control (*Neg*). **c** Western blot of immunoprecipitated samples showed equal amounts of fusion protein were purified from the cell lysates. **d** Normalized SIRT1 activities obtained at the plateau of the enzyme kinetics curve (5000–6000 s after addition of immunoprecipitates) show that the normalized SIRT1 activity observed using the purified SIRT1-fusion protein was significantly higher than that in immunoprecipitates from untransfected and SIRT1 (R446E)-fusion protein expressing cells. Immunoprecipitates isolated from untransfected cells were used as a negative control. *Asterisk* indicates the significance level of the difference between SIRT1-fusion and SIRT1 (R446E)-fusion expressing cells, *number sign* indicates the significance level of the difference between Sirt1-fusion expressing cells and untransfected cells. **e** We confirmed this finding by scrutiny of the normalized SIRT1 activity at a single time point. At 96 min (5760 s) after addition of purified SIRT1- or SIRT1 (R446E)-fusion protein samples, we found purified SIRT1-fusion protein activity to be significantly higher than the activity measured in immunoprecipitates from non-transfected cells ($P = 0.015$), as well as cells expressing the SIRT1 (R446E)-fusion protein ($P = 0.032$). There was no significant difference between the normalized fluorescence in untransfected and SIRT1 (R446E)-fusion samples at this time point ($P = 0.919$). * or #, $P = 0.01$–0.05; ** or ##, $P = 0.001$–0.01; *** or ###, $P < 0.001$; **** or ####, $P < 0.0001$, *ns* not significant

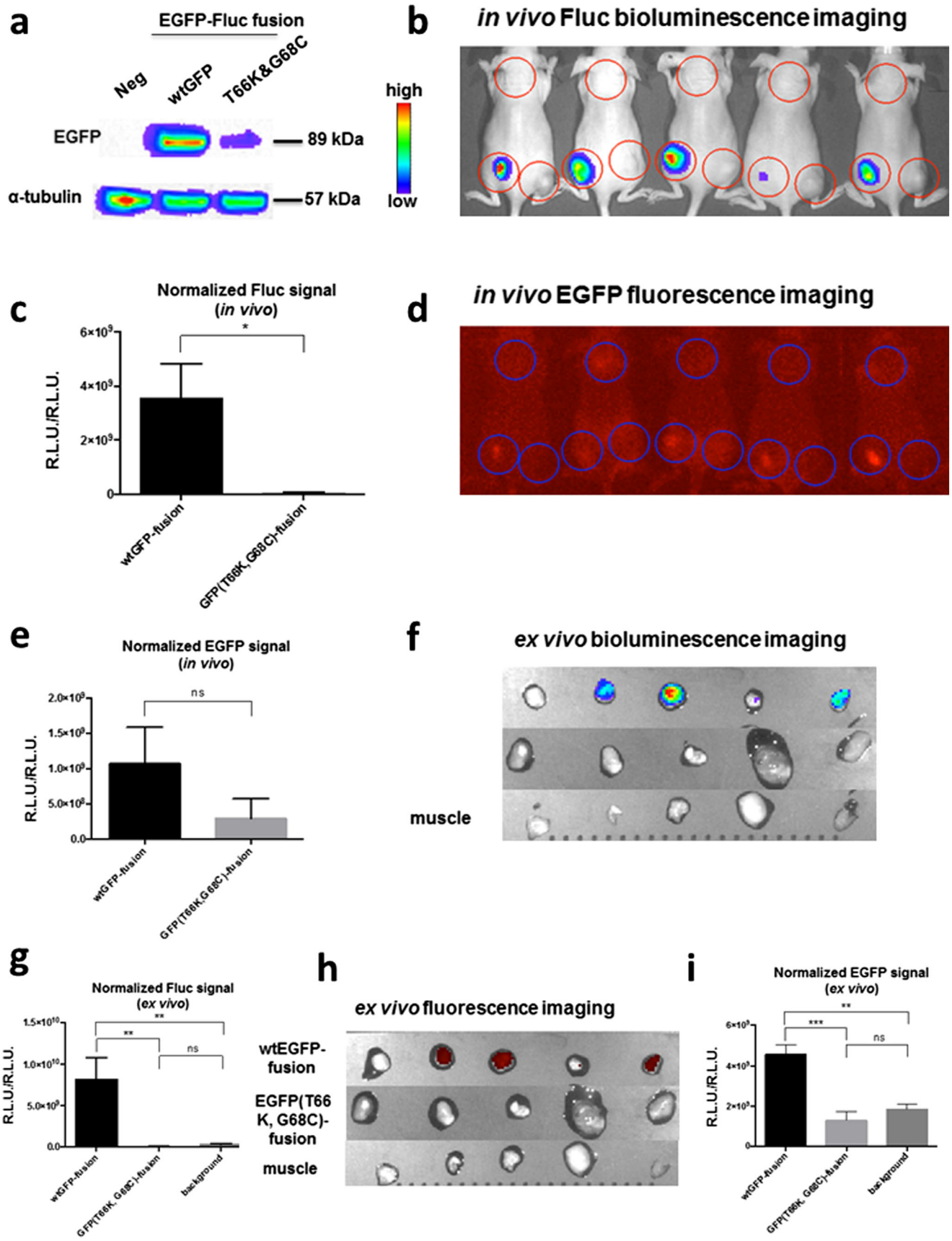
a
EGFP-Fluc fusion
Neg
wtGFP
T66K&G68C
EGFP
89 kDa
α-tubulin
57 kDa
b
in vivo Fluc bioluminescence imaging
high
low
c
Normalized Fluc signal (in vivo)
R.L.U./R.L.U.
wtGFP-fusion
GFP(T66K, G68C)-fusion
d
in vivo EGFP fluorescence imaging
e
Normalized EGFP signal (in vivo)
ns
f
ex vivo bioluminescence imaging
muscle
g
Normalized Fluc signal (ex vivo)
background
h
ex vivo fluorescence imaging
wtEGFP-fusion
EGFP(T66K, G68C)-fusion
muscle
i
Normalized EGFP signal (ex vivo)

◀ **Fig. 4** Assessment of split-Fluc biosensors by in vivo and ex vivo imaging of mice bearing HEK293T cell subcutaneous xenografts. **a** Western blot analysis of EGFP-Fluc fusion protein expression levels in cells stably expressing the wtEGFP-fusion or the mutant EGFP (T66K&G68C)-fusion proteins was used to determine the number of cells implanted in each mouse flank. **b** In vivo Fluc bioluminescence images were obtained at the experimental endpoint (18 days after implantation). Xenografts were established in the left and right flanks of nude mice using wtEGFP-fusion or EGFP (T66K&G68C)-fusion expressing cells, respectively. The scruff of the neck was used to determine background Fluc bioluminescence levels. **c** Normalized Fluc bioluminescence from the in vivo Fluc bioluminescence imaging data. **d** In vivo EGFP fluorescence images obtained at the experimental endpoint. The same regions of interest were used to obtain both in vivo Fluc bioluminescence and EGFP fluorescence data. **e** Normalized EGFP signal from the in vivo EGFP fluorescence imaging data. **f** Ex vivo Fluc bioluminescence images of wtEGFP-fusion and EGFP (T66K&G68C)-fusion expressing xenografts at the experimental endpoint (18 days after implantation). A portion of tumor-adjacent muscle was used as a negative control to determine background Fluc bioluminescence levels. **g** Normalized Fluc bioluminescence from the ex vivo Fluc bioluminescence imaging data. **h** Ex vivo EGFP fluorescence images obtained at the experimental endpoint. The same regions of interest were used to analyze both in vivo Fluc bioluminescence and EGFP fluorescence. **i** Normalized EGFP signal from the in vivo EGFP fluorescence imaging data. $*P = 0.01–0.05$; $**P = 0.001–0.01$; $***P < 0.001$; *ns* not significant

immediately after cell lysis (unpublished data). However, this tGluc recovered its activity over a few hours, which indicates that not only does the secretary signal peptide aid Gluc secretion but it also helps "rapid" intracellular Gluc folding. Generally, the duration of protein folding varies from milliseconds to minutes or hours, depending on the protein of interest and whether it is measured within or outside the cell [22]. We therefore aimed to (1) quantitate Fluc signal as it tracked the slow nascent folding of a test protein composed of Gluc truncated of its secretory signal peptide (tGluc) and (2) establish whether the two bioluminescence signals from tGluc and Fluc correlated positively. By repetitive in vitro cell lysate measurements over a 4-h period after lysis of HEK293T transiently expressing the NFLuc-tGluc-CFLuc fusion protein, we showed a strong bioluminescence activity for tGluc test protein within its biosensor, as well as a positively correlated Fluc bioluminescence signal, thus indicating Fluc fragment complementation within the biosensor that mirrors folding of the tGluc test protein Fig. 2.

Importantly, to further show the utility of the biosensor in evaluating the folding of a biologically important eukaryotic protein, rather than our light-emitting test proteins used so far, we used SIRT1. This is a class III histone deacetylase that contributes significantly to stress regulation in cells [23], and is thus involved in numerous normal intracellular processes, and in various diseases and cancers [24]. We used wild-type SIRT1 (wtSIRT1) as well as a previously reported non-functional mutant of this protein, SIRT1 (R446E) [25]. Expression vectors for wtSIRT1, SIRT1 (R446E), wtSIRT1-fusion, and SIRT1 (R446E)-fusion biosensors were delivered to HEK293T cells and analyzed. Taken together, the results shown in Fig. 3 indicate that the protein folding biosensor can be used to examine the dynamic structure-dependent function of a biologically important mammalian protein, SIRT1, in live cells.

Next, bearing in mind the future goal of using this biosensor for in vivo validation of potential new anti-misfolding drugs, we evaluated the utility of the biosensor in recording the folding status of the test protein EGFP in a mouse model (Supplementary Material and Fig. 4a–e). Fluc bioluminescence and EGFP fluorescence signals were quantified in subcutaneous xenografts placed in the flanks of nude mice by implantation of HEK293T cells stably expressing the wtEGFP-fusion or double mutant EGFP (T66K, G68C)-fusion proteins. We also harvested each tumor immediately after the final in vivo images were acquired and ex vivo imaged them in a similar fashion (Supplementary Material and Fig. 4f–i). We thus demonstrated the potential for extending the applicability and utility of this biosensor across different platforms relevant to the drug discovery process, from cell culture to an animal model, when evaluating the folding status for a particular test protein.

Many of the proteins implicated in the pathogenesis of misfolding diseases escape the diverse molecular chaperoning pathways that are in place to assist and assure the fidelity of correct protein folding. Hence, more biologically representative in vivo structural and functional studies of these abnormal events, carried out in the context of living cell environments, may be best suited to the discovery of molecular mechanisms and therapeutics to prevent or ameliorate such diseases. The development and comprehensive proof-of-principle validation of the new molecularly engineered protein folding biosensor we describe herein now pave the way for many more research directions to enable improved HTS of chemical libraries for discovery of new or repurposed anti-misfolding drugs. The application of this particular innovation to imaging in living subjects also heralds other potential far-reaching research directions that could lead for the first time to the study of protein folding in vivo, to seamless validation of anti-misfolding drugs in mouse models using the same biosensor as in HTS, and to the intriguing theoretical possibility of a similar split positron emission tomography reporter-based strategy [16] for future clinical imaging of protein folding in cell transplants in humans.

Acknowledgments We acknowledge use of the Stanford Center for Innovation in In-Vivo Imaging (SCi^3) Core Facility and thank Dr. Sanjiv Sam Gambhir, Chairman, Department of Radiology, Stanford University, for his constant support. This work was supported by the National Institutes of Health (NIH grant R21CA185805 to T.F.M. and R.P.). T.F.M. was supported in part by the Ben and Catherine Ivy Foundation.

Compliance with ethical standards

Conflict of interest The authors declare that they have no competing interests.

References

1. Denny RA, Gavrin LK, Saiah E (2013) Recent developments in targeting protein misfolding diseases. Bioorg Med Chem Lett 23: 1935–1944
2. Ong DS, Kelly JW (2011) Chemical and/or biological therapeutic strategies to ameliorate protein misfolding diseases. Curr Opin Cell Biol 23:231–238
3. Buchner J, Kiefhaber T (2008) Protein folding handbook. Wiley-VCH Verlag GmbH & Co. KGaA. Print ISBN: 9783527307845. Online ISBN: 9783527619498. Doi: 10.1002/9783527619498
4. Pittman AM, Lage MD, Poltoratsky V, Vrana JD, Paiardini A, Roncador A, Cellini B, Hughes RM, Tucker CL (2012) Rapid profiling of disease alleles using a tunable reporter of protein misfolding. Genetics 192:831–842
5. Cabantous S, Rogers Y, Terwilliger TC, Waldo GS (2008) New molecular reporters for rapid protein folding assays. PLoS One 3: e2387
6. Ebbinghaus S, Dhar A, McDonald JD, Gruebele M (2010) Protein folding stability and dynamics imaged in a living cell. Nat Methods 7:319–23
7. Schuler B, Eaton WA (2008) Protein folding studied by single-molecule FRET. Curr Opin Struct Biol 18:16–26
8. Curnow P, Booth PJ (2010) The contribution of a covalently bound cofactor to the folding and thermodynamic stability of an integral membrane protein. J Mol Biol 403:630–642
9. Deniz AA et al (2000) Single-molecule protein folding: diffusion fluorescence resonance energy transfer studies of the denaturation of chymotrypsin inhibitor 2. Proc Natl Acad Sci U S A 97:5179–5184
10. Weiss S (2000) Measuring conformational dynamics of biomolecules by single molecule fluorescence spectroscopy. Nat Struct Biol 7:724–729
11. Weissleder R, Ntziachristos V (2003) Shedding light onto live molecular targets. Nat Med 9:123–128
12. Willmann JK, van Bruggen N, Dinkelborg LM, Gambhir SS (2008) Molecular imaging in drug development. Nat Rev Drug Discov 7: 591–607
13. Christopher JA, Baldwin TO (1996) Implications of N and C-terminal proximity for protein folding. J Mol Biol 257:175–187
14. Paulmurugan R, Umezawa Y, Gambhir SS (2002) Noninvasive imaging of protein-protein interactions in living subjects by using reporter protein complementation and reconstitution strategies. Proc Natl Acad Sci U S A 99:15608–15613
15. Michnick SW (2001) Exploring protein interactions by interaction-induced folding of proteins from complementary peptide fragments. Curr Opin Struct Biol 11:472–477
16. Massoud TF, Paulmurugan R, Gambhir SS (2010) A molecularly engineered split reporter for imaging protein-protein interactions with positron emission tomography. Nat Med 16:921–926
17. Wu JC, Sundaresan G, Iyer M, Gambhir SS (2001) Noninvasive optical imaging of firefly luciferase reporter gene expression in skeletal muscles of living mice. Mol Ther 4:297–306
18. Paulmurugan R, Gambhir SS (2007) Combinatorial library screening for developing an improved split-firefly luciferase fragment-assisted complementation system for studying protein-protein interactions. Anal Chem 79:2346–53
19. Yang J, Koga Y, Nakano H, Yamane T (2002) Modifying the chain-length selectivity of the lipase from *Burkholderia cepacia* KWI-56 through in vitro combinatorial mutagenesis in the substrate-binding site. Protein Eng 15:147–152
20. Tsien RY (1998) The green fluorescent protein. Annu Rev Biochem 67:509–544
21. Topell S, Hennecke J, Glockshuber R (1999) Circularly permuted variants of the green fluorescent protein. FEBS Lett 457:283–289
22. Kubelka J, Hofrichter J, Eaton WA (2004) The protein folding 'speed limit'. Curr Opin Struct Biol 14:76–88
23. Liu T, Liu PY, Marshall GM (2009) The critical role of the class III histone deacetylase SIRT1 in cancer. Cancer Res 69:1702–1705
24. Sharma A, Gautam V, Costantini S, Paladino A, Colonna G (2012) Interactomic and pharmacological insights on human sirt-1. Front Pharmacol 3:40
25. Dai H, Case AW, Riera TV, Considine T, Lee JE, Hamuro Y, Zhao H, Jiang Y, Sweitzer SM, Pietrak B et al (2015) Crystallographic structure of a small molecule SIRT1 activator-enzyme complex. Nat Commun 6:7645